BOLETIN DE LA SOCIEDAD ESPAÑOLA DE
Cerámica y Vidrio
www.elsevier.es/bsecv

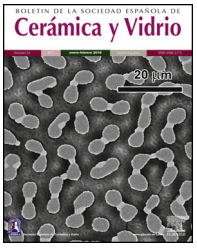

Applicability of near-field electrospinning for the development of TCP-based thin fibres and scaffold 3D printing

M. García-Galán, F.J. Martínez-Vázquez[1], *N. Rebollo-Muñoz, J.M. Montanero, P. Miranda*[*]

Universidad de Extremadura, Escuela de Ingenierías Industriales, Departamento de Ingeniería Mecánica, Energética y de los Materiales, Badajoz, Spain

ARTICLE INFO

Article history:
Received 9 March 2022
Accepted 31 May 2022
Available online 11 June 2022

Keywords:
Near-field electrospinning
UV-assisted DIW
3D printing
TCP
Scaffold

ABSTRACT

A novel method for obtaining ceramic (tricalcium phosphate, TCP) fibres with a small diameter (below 0.1 mm) is proposed and its potential use in the 3D printing of scaffolds for biomedical applications is explored. An ink consisting of a high solid content (40 vol%) ceramic slurry in a photocurable resin was prepared and extruded using near-field electrospinning. The influence of the electric potential, flow rate, and distance between tip and collector on the fabrication process in static mode were studied and the role played by unidirectional motion of the collector was also analyzed. A one order of magnitude reduction in the diameter of the jet to around 30 μm is demonstrated under static conditions, which increased to around 100 μm when collector was displaced. Continuous fibres were deposited but the slurry spread over the collector. The method was implemented on a DIW system, using in-flight UV light curing to prevent the spreading of the ink upon deposition. The feasibility of the strategy was demonstrated, although challenges remain for the optimization and control of the fabrication process. Nevertheless, these preliminary results suggest this could be a promising alternative to produce 3D ceramic scaffolds for biomedical applications with improved spatial resolution.

Aplicabilidad del electrohilado de campo cercano para la obtención de fibras delgadas basadas en TCP y la impresión 3D de andamiajes

Palabras clave:
Electrohilado de campo cercano
Moldeo robotizado asistido por luz ultravioleta

RESUMEN

Se propone un nuevo método para la obtención de fibras cerámicas (fosfato tricálcico, TCP) de pequeño diámetro (menos de 0.1 mm) y se explora su potencial uso en la impresión 3D de andamiajes para aplicaciones biomédicas. Suspensiones cerámicas de alto contenido sólido (40 vol%) en una resina fotocurable fueron extruidas mediante electrohilado de campo cercano, analizando la influencia del potencial eléctrico, el caudal y la distancia entre la

[*] *Corresponding author.*
E-mail address: pmiranda@unex.es (P. Miranda).
[1] Currently at Universidad de Sevilla, Facultad de Física, Departamento de Física de la Materia Condensada, Avda. Reina Mercedes s/n, 41012 Seville, Spain.

https://doi.org/10.1016/j.bsecv.2022.05.003

Impresión 3D
TCP
Andamiaje

punta y el colector y el movimiento de este en el diámetro de la fibra. Se demuestra una reducción de un orden de magnitud en el diámetro del chorro hasta ~30 μm en estático y hasta ~100 μm con el colector en movimiento. Se depositaron fibras continuas, pero se observó esparcimiento de la suspensión sobre el colector. El método se implementó en un sistema de moldeo robotizado, utilizando curado en vuelo por luz ultravioleta para evitar el esparcimiento de la tinta tras la deposición. Aunque la viabilidad de la estrategia queda demostrada, siguen existiendo retos para la optimización y control del proceso de fabricación. No obstante, estos resultados preliminares indican que esta técnica podría ser una alternativa prometedora para producir andamios cerámicos 3D para aplicaciones biomédicas con una resolución espacial mejorada.

Introduction

Thin ceramic fibres, due to their high surface to volume ratio and superior strength, are widely used in variety of applications ranging from catalysis [1,2] to biomedical materials [3,4], and, especially, in the fabrication of composites with enhanced mechanical properties, both in terms of strength and fracture toughness [5]. The production of ceramic fibres has grown exponentially in the recent years and, among the different techniques devoted to their production, electrospinning stands out as one of the most suitable for producing continuous nanofibres with variable fibre dimensions. Typically, this process takes place by using a liquid preceramic polymer solution that is ejected through a metallic nozzle at a constant flow rate with the aid of a strong electric field. Under these conditions, the sol forms a liquid meniscus from whose tip a jet, with a diameter significantly smaller than the nozzle, is emitted. The solvent eventually evaporates, and the resulting fibre is deposited on a collector in a randomly oriented disposition. The selection of the fabrication parameters (electric potential, distance tip-collector, flow rate, collector nature, etc.) has a significant influence on the fibre features. Nonetheless, electrospinning applications are relegated to 2D materials, such as membranes for electrical devices [6], filtration [7] or biomedical [8–10] purposes, where the precise control on the fibre location is generally trivial. Also, there are limitations in the ceramic compositions that can be produced in this way and the relatively low yield of the process can limit its scaling up.

Recently, it has been shown that, in the case of scaffolds for bone regeneration, it is beneficial to have regular, highly interconnected network of pores and struts, in order to optimize their biological and, especially, their mechanical performance [11,12]. Being able to accurately control their external 3D shape to fit the patient lesion is also desirable. Direct Ink Writing (DIW) is becoming an additive manufacturing (AM) technique of choice to fabricate scaffolds with all these desirable features from bioactive materials like calcium phosphates [13,14] or bioglasses [15–17]. However, one of the main limitations of this AM technique is that clogging of the extrusion nozzle prevents the production of thin ceramic struts, which are then typically over 200 μm in diameter. Overcoming this limitation is of great importance since one of the main drawbacks of bioceramic scaffolds is their low strength. In this sense, a simple way to increase the scaffolds strength, without adding additional polymeric phases [18–20], would be to reduce the diameter of the bioceramic struts. In this way, Weibull size effect [21], associated to a reduction in the population of large precursor defects responsible for the fracture, would produce an increase in the ceramic rod intrinsic strength and, consequently, improve the overall strength of the scaffold.

Combining electrospinning with DIW is proposed here as a suitable solution to overcome the limitations of both techniques and take advantage of their most attractive features for producing scaffolds with enhanced performance. In Near-Field Electrospinning (NFE) [22–24], the collector is a flat surface (substrate) on which the electrospun polymeric fibre is gently deposited in a controlled way by considerably reducing the tip-to-substrate distance during the deposition process. This eliminates the whipping instability in the jet, caused by the electric field, which leads to the randomly bent fibres [25]. Here, we propose using a strategy consisting in using a modified DIW device for producing NFE of a ceramic slurry in a photosensitive polymer (instead of a polymer solution) to produce thin bioceramic fibres and 3D printed scaffolds. The idea is to produce a significantly stretched jet by adding an electrical field and then using UV light to cure the deposited fibre to preserve its position and shape enabling a layer-by-layer build-up of 3D structures. To the best of our knowledge, this combination of techniques (DIW, NFE and UV-photocuring) has never been explored before. Thus, beside implementing the appropriate deposition system, numerous process parameters (optimal ink composition, voltage, nozzle-collector distance, printing speed, UV-light intensity, etc.) would have to be optimized in order to enable the additive manufacturing of ceramic scaffolds with enhanced resolution, surface roughness and mechanical strength. In this work, we provide a proof of concept of the viability of this method and analyze the influence of various fabrication process parameters on the resulting fibre dimensions.

Materials and methods

Preparation and characterization of slurry

Commercial powder of β-tricalcium phosphate (TCP) with an average particle size of 2.98 μm (Whitlockite OD, Plasma Biotal Ltd.) was combined with oleic acid (Sigma Aldrich,

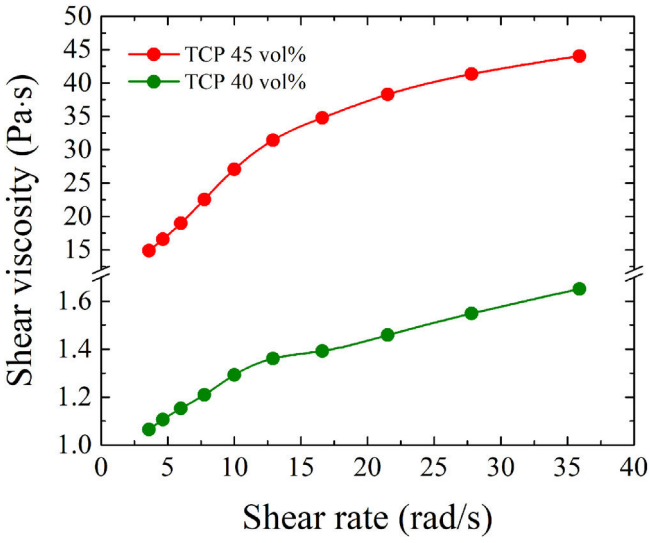

Fig. 1 – Shear viscosity versus shear rate for TCP-based photocurable slurries with the indicated solid contents.

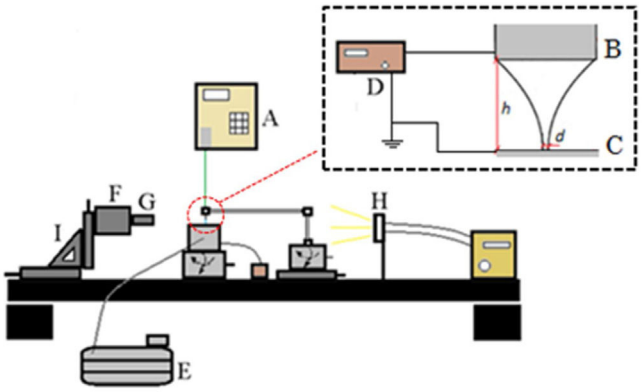

Fig. 2 – Sketch of the setup for the experiments in the static mode. (A) Syringe pump, (B) tip, (C) collector, (D) power supply, (E) suction pump, (F) camera, (G) optical lenses; (H) UV filter, and (I) triaxial translation stage.

Germany) as a dispersant in a proportion of 0.1 wt% relative to the amount of TCP. Both components were mixed in ethanol by stirring for 2 h and the solvent was subsequently evaporated before further use. In parallel, a mixture of photocurable resin (FTD Standard Blend 3D Printing resin, Fun to Do, Alkmaar) and camphor (Sigma Aldrich, Germany) was prepared in a weight ratio of 70:30. The addition of camphor helps reducing the viscosity of the ink [26] resulting from adding the prepared powder to the mixture. The resulting slurry was homogenized in a centrifugal mixer (ARE-250, THINKY Corop., Tokyo, Japan) for 4 min at 1200 rpm, including a few 5 mm alumina balls to break any agglomerates. The photocurable inks were stored in an opaque container at room temperature during and after preparation. The viscosities of the resulting inks were measured with a rheometer (DHR-2, TA Instruments) by performing a flow sweep test in a concentric cylinder geometry. Viscosity values were collected for a range of shear rates from 3.59 to 35.9 rad/s and, as shown in Fig. 1, the viscosity increased dramatically when increasing solid content above 40 vol%, so this concentration was adopted as the optimal for all subsequent experiments. Both slurries showed a dilatant behaviour which, although suboptimal for extrusion applications, is not uncommon for ceramic filled polymeric resins such as those used in dental applications. The electrical conductivity of such ink was measured with a picoammeter (Keithley 6485), a power supply (HQ Power PS3003) and an insulating tube that contained the sample. Two screws connected on the extremes of the tube were used as electrodes as described elsewhere [27]. Current intensity values were registered for potentials from 0 to 30 V in steps of 5 V and the conductivity was calculated from the slope of the linear fit to the voltage-intensity data collected, resulting in a mean value of 4.96×10^{-7} S/m.

Experimental setup

Three different experimental setups were used in order to determine the optimal conditions for fibre production, collection, and 3D printing: a fully static setup, a static nozzle with moving substrate and a moving 3D printing nozzle over static substrate. The static setup is optimal for the characterization of the jets, as it produces straight filaments, while the other two setups are relevant to the practical applications of fibre collection and the printing of 3D objects, respectively.

In order to determine the optimal conditions leading to a stable production of jets, a preliminary study was conducted under static conditions (i.e., with both the tip and collector at rest) using the set-up schematized in Fig. 2. A syringe filled with a proper amount of the prepared ink was coupled to a syringe pump (Harvard Apparatus PDH 4400) to generate a constant flow of ink during the experiments. A tube was connected to the syringe in one of its ends, while the other was placed vertical with the help of a gripper. A metallic tip was screwed to the tube, and a metallic collector was placed under the tip. The tip and collector were connected to a power supply (Bartan 205B-10R) to generate the desired potential difference. A hole, 1 mm in diameter, was drilled in the collector to evacuate the ink—with the help of a suction pump (Hanning Elektro-Werke SV 1003 D000) that creates an air current focusing the jet on the hole to facilitate the process—avoiding its accumulation under the tip in the motionless substrate, which would perturb the jet dynamics. A camera (Pulnix TM 1045 GE) was placed in front of the tip for the correct observation and measurement of the jet. A set of optical lenses (Goyo Optical Inc., GMHR35028MCN) was coupled to the camera to measure the jet diameter. The magnification was such that each pixel dimension was 4.54 μm. A UV filter was installed to avoid the ink polymerization during the experiment. The precise manipulation of the camera, tip and collector was achieved by a three-axis translation system (Thorlabs PT3).

To study the deposition of fibres in one dimension the previous set-up was modified (see Fig. 3) by replacing the collector used in the static mode by an aluminium plate mounted on a one-axis motorized belt. The belt was programmed by Arduino and controlled by Matlab (Matlab R2014b, MathWorks, Inc.). A UV lamp (Lantern 2-in-1 led flashlight 5 W, Morpilot, EEUU) was used to produce the polymerization of the jet right after its deposition on the tape. The UV beam was carefully focused

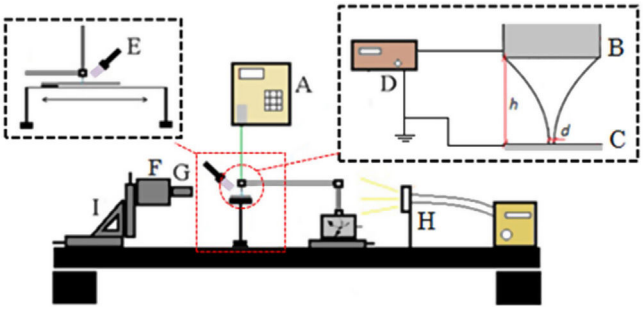

Fig. 3 – Sketch of the setup for the experiments in the dynamic mode. (A) Syringe pump, (B) tip, (C) collector, (D) power supply, (E) UV lamp, (F) camera, (G) optical lenses; (H) UV filter, and (I) triaxial translation stage.

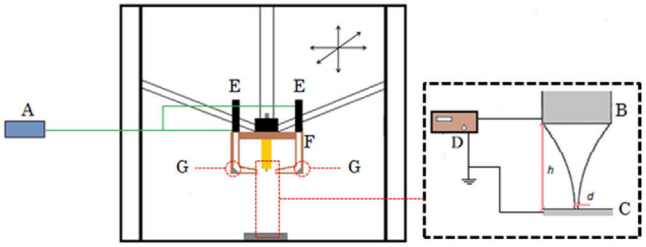

Fig. 4 – Sketch of the setup for the 3D printing experiments performed on a delta 3D printer (Delta WASP 2040 PRO, WASP, Italy) modified for DIW and including a couple of UV lasers for ink photocuring: (A) arduino controller, (B) tip, (C) collector, (D) power supply, (E) UV laser, (F) supports, (G) oblique mirrors.

on the deposition point to prevent the curing of the polymer near the meniscus tip, which would clog the nozzle. Copper (19 mm × 3.66 m × 0.09 mm, Ted Pella Inc., EEUU) and polytetrafluoroethylene (12 mm × 0.075 mm × 12 m, Unecol, Spain) tapes were used to cover the aluminium plate and collect the fibres in order to evaluate the effect of collector surface properties on the fibre morphology. Using tapes facilitated removal of the fibres from the collecting surface and rapid reusability of the substrate.

Finally, a high-speed delta 3D printer (Delta WASP 2040 PRO, WASP, Italy) was modified to be suitable for DIW and a couple of UV lasers (NEJE module 3500, Shenzhen Zhixinjie Technology Co., China) systems, as schematized in Fig. 4, were added for photocuring the developed inks. The system was used to test the feasibility of the proposed method for the fabrication of 3D structures layer by layer.

Scanning electron microscopy (S-3600N, Hitachi, Japan) was used to determine the morphology and fibre dimensions of fabricated samples, previous metallization with platinum using a PVD device (SC 7640, Polaron Range, Germany). A qualitative analysis of the chemical composition of the fibre was also performed by energy dispersive X-ray analysis (EDX, Quantax 400, Bruker).

Results and discussion

Static experiments

The effect of various experimental parameters on the filaments produced by electrospinning of the developed ceramic slurry was first analyzed in static mode. Specifically, the influence of the distance *h* between the collector and the tip on the applied voltage *V* necessary to obtain a stable and homogeneous jet was examined, as well as the variation of the jet diameter *d* with the distance *h*, the voltage *V*, and the injected flow rate Q. This analysis enabled the determination of the optimal conditions for the production of a stable jet with minimum diameter. We conducted experiments using several nozzle diameters, but the best results were obtained with a tip of 0.33 mm inner diameter (i.e., that was the minimum diameter that allowed uninterrupted flow of the photocurable inks developed without any eventual clogging issues). Thus, all the experiments presented in this section were conducted with that tip.

Fig. 5a shows the relationship between the applied voltage *V* and the tip-to-collector distance *h* for stable jet emission. The experiments were conducted for Q = 0.5 ml/h, the minimum flow rate for which steady ejection took place. As can

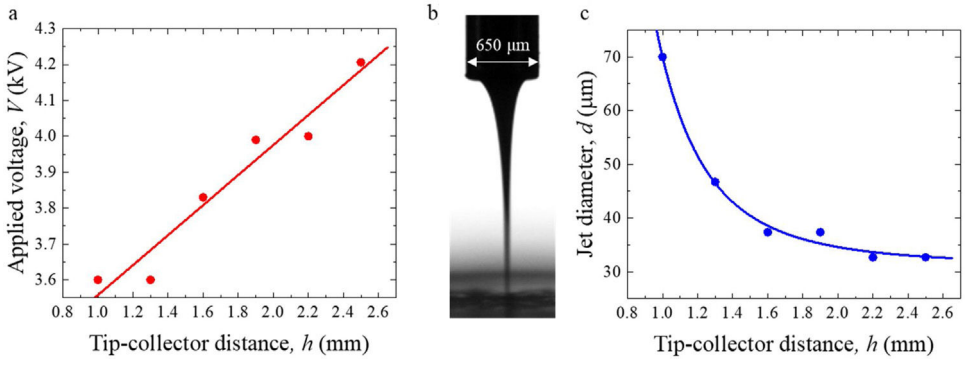

Fig. 5 – Result of static experiments for the minimum Q = 0.5 ml/h: (a) plot of the minimum applied voltage *V* required to produce a stable jet versus the tip-to-collector distance *h*; (b) optical image of a stable jet produced in such experiments; and (c) plot of the evolution of the jet diameter *d* versus the tip-to-collector distance *h* at such minimum voltages. Lines in the plots are just included as eye-guides.

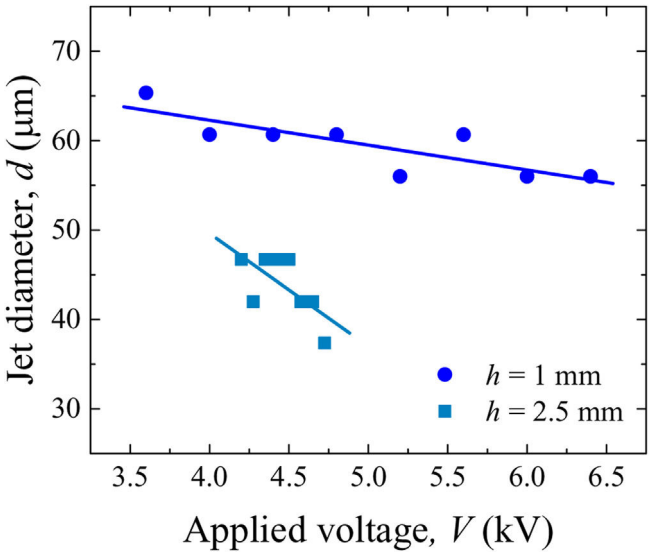

Fig. 6 – Jet diameter *d* versus the applied voltage V for Q = 0.5 ml/h at the indicated collector-tip distances *h*. Lines in the plots are just included as eye-guides.

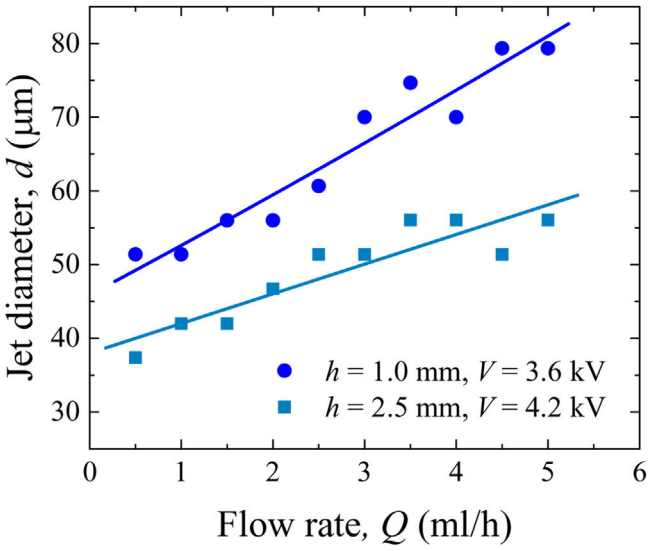

Fig. 7 – Jet diameter *d* versus the injected flow rate Q at the indicated collector-tip distances and applied voltages. Lines in the plots are just included as eye-guides.

be expected, the voltage increases with *h*, so that an electric field with sufficient intensity is applied. However, the relative increase of *V* is much smaller than that of the distance *h*. For instance, when *h* is increased by a factor of 2.5 (150%), the voltage *V* increases only around 15%. This means that the intensity of the electric field ($E \approx V/h$) needed to maintain the jet emission decreases as *h* increases, probably because the electric field becomes more aligned with the jet as the tip is moved away from the collector. For $h > 2.5$ mm, the whipping instability typical of conventional electrospinning occurred. This instability is caused by the instantaneous re-distribution of charge along a portion of the jet surface when that portion moves slightly off-axis [25]. This charge displacement produces electrical forces pushing the jet farther away from its axis, which provokes jet bending. The violent slashes characterizing this whipping regime either end up breaking the jet or, at the very least, precludes a gentle, controlled deposition on the collector. However, below that value of the distance *h*, stable jets could be produced, as shown in Fig. 5b. The jet diameter *d* was found to steadily decrease (Fig. 5c) with the distance *h* to the collector for a constant flow rate of Q = 0.5 ml/h and the minimum required applied voltages. However, the decrease is far sharper for $h < 1.6$ mm, with the jet diameter remaining practically constant as the tip is brought farther than that value from the collector. For the smaller *h* values, the jet touches the collector before the stretching process is completed, which explains the dramatic diameter increase. The jet diameter is brought down to around 30 μm for $h > 1.6$ mm, which constitutes an order of magnitude reduction with respect to the tip diameter (330 μm).

As shown in Fig. 6, when the rest of parameters are fixed, the applied voltage has little influence on *d*, as typically occurs in electrospray: once the voltage is properly selected to produce the so-called cone-jet mode, it has a small effect on the outcome [28]. The effect seems to be somewhat more pronounced at the larger tip-collector distance ($h = 2.5$ mm). However, the range of voltages that enables the production of stable jets (without whipping) at that distance is substantially reduced, so in either case the diameter cannot be modified by more than 10 μm just by changing the applied voltage. On the contrary, the injected flow rate Q significantly influences the jet diameter (Fig. 7). As Q decreases, the energy per unit mass transferred by the electric field to the liquid increases. Consequently, the jet velocity increases and, therefore, its diameter decreases. The observed dependence of *d* on Q (Fig. 7) does not seem to follow, however, the scaling law $d \propto Q^{1/2}$ typically verified by low-viscosity liquids [28,29]. As expected, for all the injected flow rates, the jet diameter is substantially lower when the distance *h* is increased. All these results yield $h = 1.6$–2.5 mm, a voltage of $V = 3.8$–4.7 kV (depending on the selected distance), and Q = 0.5 ml/h as optimum values for steadily producing the thinnest jets under static conditions.

Dynamic experiments

Once these conditions were established, the role played by the collector movement and material for the optimum fibre deposition was analyzed. The fibre resulting from the jet solidification, upon application of a curing UV-light that was added in this new setup (see Fig. 3), could not be properly deposited on the moving substrate for the optimal parameters determined under static conditions. Moreover, for $h > 1.6$ mm, the traction force exerted by the substrate destabilized the jet emission for all the substrate speeds considered in our experiments (30–80 mm/s), as occurs in the draw resonance instability in fibre spinning [30]. And even at such reduced distance ($h = 1.6$ mm), the jet broke up when touching the substrate when $Q < 2$ ml/h. Thus, $h = 1.6$ mm and Q = 2 ml/h were found to be the optimum distance and flow rate to deposit the fibre on the moving substrate. We conducted experiments covering the substrate with copper and

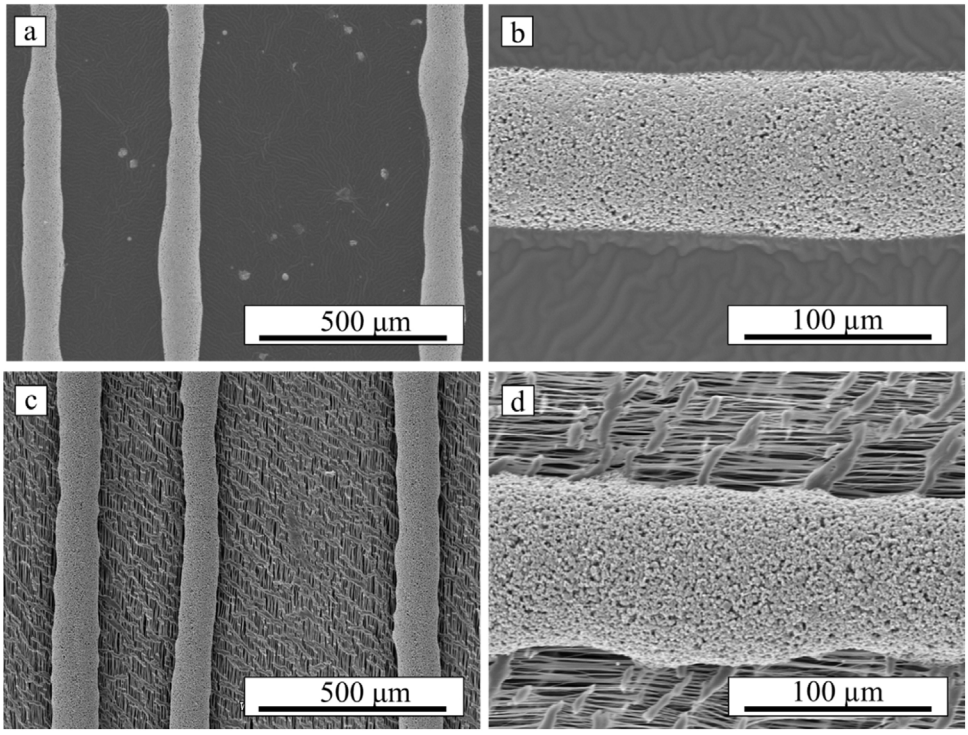

Fig. 8 – SEM images of fibres deposited on (a, b) copper and (c, d) PTFE.

polytetrafluoroethylene (PTFE) tapes. For PTFE tape a voltage similar to the optimal value for the static experiments (V = 4 kV) was applied between the tip and the moving substrate. However, use of a copper tape significantly altered the electric field and the voltage had to be decreased to 2 kV to stabilize the jet emission and avoid whipping. The substrate speed was gradually varied to determine its effect on the quality of the fibre deposited. For both substrates, the best deposition (minimal fibre diameter with reasonable uniformity) was obtained for a substrate speed of 60 mm/s.

With the above choice of the control parameters, fibres were continuously deposited on both moving substrates (Fig. 8). The fact that the deposition was conducted without loss of continuity is of great relevance for any future applications of the proposed fabrication method, including 3D printing. When the collector was covered with copper (Fig. 8a and b) deposited fibres exhibited some lack of uniformity and a relatively large width at some points; and appeared flattened onto the substrate. Indeed, despite producing jet diameters as small as $d \approx 45$ μm, the average width of the deposited fibres lied around 150 μm. This indicates that curing of the fibres was insufficient or occurred well after deposition, which allowed the liquid to spread as it wetted the substrate. As confirmed by energy dispersive X-ray analysis, the chemical composition of the fibre was very homogeneous, with no evidence of segregation between the photocurable resin and the powder. The fibres exhibited a roughness and porosity (Fig. 8b) similar to that of scaffolds manufactured by photo-curing of similar inks using the digital light processing (DLP) technique [31]. As can be observed in Fig. 8c and d, fibres that are thicker in the direction perpendicular to the substrate and somewhat less wide (≈100 μm on average) may be printed in the case of a moving PTFE substrate. This can be explained in terms of polytetrafluoroethylene hydrophobicity and rugosity, which hindered ink spread and wetting of the substrate. However, the fibre morphology became more irregular than on the copper-covered substrate owing to the surface rugosity of the PTFE tape (cf. Fig. 8b and d). However, although this solution to avoid ink spreading could be feasible when producing individual ceramic fibres, it would only affect the first layer on a 3D printing construct. Therefore, increasing the level of curing prior to deposition on the substrate is required to enable a proper superposition of subsequent layers of fibres in 3D printing.

Some preliminary tests were performed using the system schematized in Fig. 4 to evaluate the feasibility of the proposed method for 3D printing, using two UV lasers as light sources to better focus the illuminated area and to accelerate photocuring prior to deposition. Several layers were deposited in each experiment with the purpose of trying to build a 3D structure and the 3D printing parameters and lighting conditions were adjusted. An aluminium substrate, with very similar behaviour compared to the copper plate, was used in this case as a collector to provide a wider area for two-dimensional movement. Soon a critical aspect related to the application of the intense UV lighting required to produce curing prior to deposition was identified: the hardening of the ink in the Taylor cone area during printing due to unwanted reflections of ultraviolet light in the substrate. It should be noticed that the residence time of the fluid in the Taylor cone is much larger than that in the jet, which favours ink hardening in the cone. The accumulation of hardened ink in the cone/nozzle as the printing progresses eventually leads to the collision of such crust with the printed layers and/or the generation of

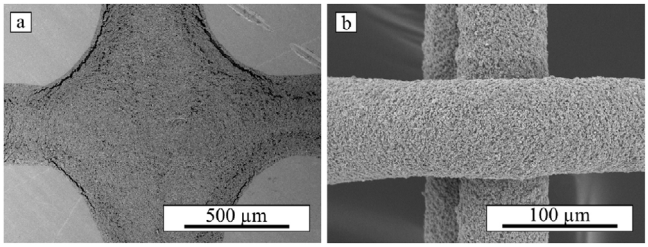

Fig. 9 – SEM image of the intersection of fibres deposited orthogonally in different layers under (a) low and (b) high UV exposure.

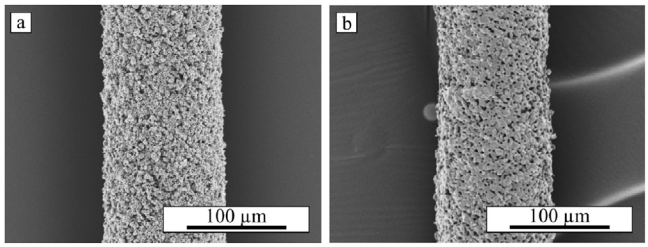

Fig. 10 – SEM images of a typical fibre deposited by NFE UV-assisted DIW (a) before and (b) after sintering.

an electric arc. That is why in the final setup depicted in Fig. 4 the UV light was made to hit the jet horizontally, through the use of inclined mirrors, and collimated as much as possible before reaching the jet. In order to prevent the collision of the devised holder setup with already deposited, the tip-collector distance had to be increased to $h = 6$ mm: larger distances would make it harder to obtain continuous lines. At this distance, the voltage (V) necessary to obtain a stable jet was increased to 6000 V. Flow rate, Q, had to be adjusted too. In the 3D printer this is controlled by various parameters that can be selected in the Ultimaker Cura control software employed: nozzle size, line width, flow parameter. Optimal results in our preliminary experiments were 0.32 mm for the nozzle and line width, and 20% for the flow parameter, which produced sufficient flow rate to avoid loss of continuity in the deposited fibres. Adjusting the printing speed enabled a variation of the diameter of the jet and the resulting deposited fibres and, as will be discussed later, this implies certain limitations for the proposed 3D printing technique. Speeds ranging from 350 to 500 mm/s were successfully used to produce printed fibres of various widths.

However, there are several aspects related to the application of UV light in the jet itself that make this technique hard to use and can affect the reproducibility of its results. As shown in Fig. 9a, when the UV beam is focused on the region of the jet right before it reaches the substrate, an insufficient curing of the resin is produced, and the deposited fibres collapse on top of each other, preventing the correct layer stacking required to build the 3D structure. This can be solved by focusing the UV laser beam upstream, although care needs to be taken to remain far enough to the Taylor cone to avoid the clogging of the tip. When successfully done, the resin is cured and the fibres preserve their shape upon deposition, making it possible to stack several layers (Fig. 9b). This implies a far better scenario than the latter (Fig. 9a) for a correct 3D printing process, but still presents issues since there was a significant lack of adhesion between deposited layers, which is a critical issue that must be addressed for a successful additive manufacturing process using the proposed methodology. Moreover, at the position selected for those tests, the Taylor cone can still harden and clog the nozzle overtime unless very high printing speeds, close to the top speed of the system (500 mm/s), are used. Around the maximum speed Taylor cone hardening occurs far less frequently due to a lower exposure to UV light as a consequence of the faster flow of the ink. However, using such high printing speeds produce significant stretching of the filaments which, while good for reducing the final diameter of the deposited fibres, make it harder to control the stability of the deposition process. Larger variations on the fibre diameter were observed and loss of continuity defects can more easily appear. Moreover, when the printing head approaches an edge of the print, it has to slow down for a short time to change direction while the ink continues to flow at similar rate and the UV light continues to hit the jet with the same intensity. This causes that at any change in the direction of print the jet increases its diameter and is exposed longer to the UV-light producing an engrossment of the fibres and greater fibre contraction upon curing, typically resulting in detachment from the substrate and curling of the fibres at the edges of the print. As the printing progresses, the nozzle eventually collides with these lifted and curled fibres and the 3D printing fails. This problem becomes more severe the smaller the sample to be printed is. None of the printing parameters that could be modified helped to overcome this problem.

Further work using systems with better means for dynamically controlling the intensity of the UV-light, printing speed and ink flow, as well as better systems for protecting the sensitive Taylor cone from the UV light, would be needed for the successful implementation of the proposed methodology (NFE plus UV-assisted DIW) as a reliable 3D printing system for ceramic materials with improved spatial resolution. Also, UV-dose received by the emitted jet will have to be fine-tuned in order to achieve a suitable level of shape retention while still allowing the deposited fibres in adjacent layers to bond together to construct the desired 3D part.

Despite the aforementioned limitations, this initial study has demonstrated beyond a doubt that the proposed fabrication process is suitable for obtaining individual fibres or simple meshes comprised of thin ceramic fibres, which as shown in Fig. 10 can reach under 80 μm, especially after sintering. The reduction in the fibre diameter shown in this figure is not too large due to the relatively low sinterability of TCP [31] (note the high level of porosity remaining after sintering, Fig. 10b). Therefore, even smaller dimensions could be achieved if a fully densifiable ceramic material was used in the ink. Moreover, as shown in the static tests, the proposed methodology has the potential to get to even smaller jet diameters and therefore final feature dimensions. Undoubtedly, future efforts must still be carried out to find the optimal conditions of this technique to be considered for additive manufacturing of 3D specimens, but this work establishes a firm starting point for

a promising strategy to build a new generation of ceramic parts.

Concluding remarks

A proof of concept of the viability of a novel technique, based on the NFE of ceramic (TCP) photocurable slurries, for manufacturing homogeneous, thin ceramic-based rods is provided in this study. The results obtained demonstrate also that these rods could be used to construct bioceramic scaffolds for bone regeneration by combining NFE with UV-assisted DIW. The influence of the injected flow rate, the tip-to-substrate distance, and the applied voltage on the diameter of the slurry jet produced was analyzed. The role of substrate movement and surface properties (copper vs. polytetrafluoroethylene) on the morphology of the deposited fibres were examined as well. A preliminary experimental setup for the implementation of a system using NFE and UV-Assisted DIW (or UV- and electrospinning-assisted direct ink writing, UVE-DIW) was built and the optimal printing parameters to deposit a mesh comprising several layers of thin bioceramic fibres were determined.

Although several limitations regarding the UV lighting conditions and the level of photocuring induced on the deposited ink were identified, the results presented in this work are very promising. Specifically, meshes were obtained with strut/fibre sections well below what can be achieved with any traditional extrusion-based methods, such as DIW or FFF, paving the way for the production of ceramic-based structures with smaller dimensional features and enhanced resolution. This could be of special interest for producing bioceramic tissue engineering scaffolds and ceramic filtration systems with smaller pore sizes, were even high resolution techniques like SLA/DLP struggle due to difficulties in the elimination of residual slurry trapped within small pores [32]. The production of porous bioceramic scaffolds with smaller strut diameters could also lead to enhanced strength due to a Weibull size effect. Although such extreme would have to be validated in future works, this could provide a means to the fabrication of mechanically sound bioceramic scaffolds suitable for load-bearing applications.

Acknowledgements

This work was supported by grants RTI2018-095566-B-I00, PID2019-108278RB-C32 and PEJ2018-003586-P funded by MCIN/AEI/10.13039/501100011033 and co-funded either by the European Regional Development Fund (ERDF, a way to make Europe) or the European Social Fund (FSE invest in your future). Financial support from Junta de Extremadura (through grants no. GR18149 and GR18175) is also gratefully acknowledged.

REFERENCES

[1] L. Yin, J. Niu, Z. Shen, Y. Bao, S. Ding, Preparation and photocatalytic activity of nanoporous zirconia electrospun fiber mats, Mater. Lett. 65 (2011) 3131–3133, http://dx.doi.org/10.1016/J.MATLET.201106092.

[2] R. Ruiz-Rosas, J. Bedia, J.M. Rosas, M. Lallave, I.G. Loscertales, J. Rodríguez-Mirasol, T. Cordero, Methanol decomposition on electrospun zirconia nanofibers, Catal. Today 187 (2012) 77–87, http://dx.doi.org/10.1016/j.cattod.2011.10.031.

[3] G. Cadafalch Gazquez, H. Chen, S.A. Veldhuis, A. Solmaz, C. Mota, B.A. Boukamp, C.A. Van Blitterswijk, J.E. Ten Elshof, L. Moroni, Flexible yttrium-stabilized zirconia nanofibers offer bioactive cues for osteogenic differentiation of human mesenchymal stromal cells, ACS Nano 10 (2016) 5789–5799, http://dx.doi.org/10.1021/acsnano.5b08005.

[4] T. Wang, J.K.H. Tsoi, J.P. Matinlinna, A novel zirconia fibre-reinforced resin composite for dental use, J. Mech. Behav. Biomed. Mater. 53 (2016) 151–160, http://dx.doi.org/10.1016/J.JMBBM.201508018.

[5] S. Feih, J. Wei, P. Kingshott, B.F. Sørensen, The influence of fibre sizing on the strength and fracture toughness of glass fibre composites, Compos. A: Appl. Sci. Manuf. 36 (2005) 245–255, http://dx.doi.org/10.1016/J.COMPOSITESA.200406019.

[6] X. Zhang, L. Ji, O. Toprakci, Y. Liang, M. Alcoutlabi, Electrospun nanofiber-based anodes, cathodes, and separators for advanced lithium-ion batteries, Polym. Rev. 51 (2011) 239–264, http://dx.doi.org/10.1080/15583724.2011.593390.

[7] K. Desai, K. Kit, Effect of spinning temperature and blend ratios on electrospun chitosan/poly(acrylamide) blends fibers, Polymer (Guildf.) 49 (2008) 4046–4050, http://dx.doi.org/10.1016/J.POLYMER.200807012.

[8] T.J. Sill, H.A. von Recum, Electrospinning: applications in drug delivery and tissue engineering, Biomaterials 29 (2008) 1989–2006, http://dx.doi.org/10.1016/J.BIOMATERIALS.200801011.

[9] M.V. Jose, V. Thomas, K.T. Johnson, D.R. Dean, E. Nyairo, Aligned PLGA/HA nanofibrous nanocomposite scaffolds for bone tissue engineering, Acta Biomater. 5 (2009) 305–315, http://dx.doi.org/10.1016/J.ACTBIO.200807019.

[10] R. Murugan, S. Ramakrishna, Development of nanocomposites for bone grafting, Compos. Sci. Technol. 65 (2005) 2385–2406.

[11] P. Miranda, A. Pajares, E. Saiz, A.P. Tomsia, F. Guiberteau, Mechanical properties of calcium phosphate scaffolds fabricated by robocasting, J. Biomed. Mater. Res. A 85A (2008) 218–227.

[12] F. Martínez-Vázquez, A. Pajares, P. Miranda, Effect of the drying process on the compressive strength and cell proliferation of hydroxyapatite-derived scaffolds, Int. J. Appl. Ceram. Technol. 14 (2017), http://dx.doi.org/10.1111/ijac.12755.

[13] P. Blázquez-Carmona, J.A. Sanz-Herrera, F.J. Martínez-Vázquez, J. Domínguez, E. Reina-Romo, Structural optimization of 3D-printed patient-specific ceramic scaffolds for in vivo bone regeneration in load-bearing defects, J. Mech. Behav. Biomed. Mater. 121 (2021) 104613, http://dx.doi.org/10.1016/J.JMBBM. 2021.104613.

[14] P. Miranda, E. Saiz, K. Gryn, A.P. Tomsia, Sintering and robocasting of β-tricalcium phosphate scaffolds for orthopaedic applications, Acta Biomater. 2 (2006), http://dx.doi.org/10.1016/j.actbio.2006.02.004.

[15] S. Eqtesadi, A. Motealleh, P. Miranda, A. Pajares, A. Lemos, J.M.F. Ferreira, Robocasting of 45S5 bioactive glass scaffolds for bone tissue engineering, J. Eur. Ceram. Soc. 34 (2014) 113–124, http://dx.doi.org/10.1016/j.jeurceramsoc.2013.08.003.

[16] A.M. Deliormanli, M.N. Rahaman, Direct-write assembly of silicate and borate bioactive glass scaffolds for bone repair, J. Eur. Ceram. Soc. 32 (2012) 3637–3646, http://dx.doi.org/10.1016/j.jeurceramsoc.2012.05.005.

[17] S. Eqtesadi, A. Motealleh, A. Pajares, P. Miranda, Effect of milling media on processing and performance of 13-93 bioactive glass scaffolds fabricated by robocasting, Ceram. Int. 41 (2015), http://dx.doi.org/10.1016/j.ceramint.2014.09.071.
[18] F.J. Martínez-Vázquez, F.H. Perera, P. Miranda, A. Pajares, F. Guiberteau, Improving the compressive strength of bioceramic robocast scaffolds by polymer infiltration, Acta Biomater. 6 (2010), http://dx.doi.org/10.1016/j.actbio.2010.05.024.
[19] C. Paredes, F.J. Martínez-Vázquez, A. Pajares, P. Miranda, Novel strategy for toughening robocast bioceramic scaffolds using polymeric cores, Ceram. Int. 45 (2019), http://dx.doi.org/10.1016/j.ceramint.2019.06.175.
[20] F.J. Martínez-Vázquez, P. Miranda, F. Guiberteau, A. Pajares, Reinforcing bioceramic scaffolds with in situ synthesized ε-polycaprolactone coatings, J. Biomed. Mater. Res. A 101 (2013) 3551–3559, http://dx.doi.org/10.1002/jbm.a.34657.
[21] W. Weibull, A statistical distribution function of wide applicability, J. Appl. Mech. ASME 18 (1951) 293–297.
[22] D. Sun, C. Chang, S. Li, L. Lin, Near-field electrospinning, Nano Lett. 6 (2006) 839–842, http://dx.doi.org/10.1021/nl0602701.
[23] X.-X. He, J. Zheng, G.-F. Yu, M.-H. You, M. Yu, X. Ning, Y.-Z. Long, Near-field electrospinning: progress and applications, J. Phys. Chem. C 121 (2017) 8663–8678, http://dx.doi.org/10.1021/acs.jpcc.6b12783.
[24] P. Fattahi, J.T. Dover, J.L. Brown, 3D near-field electrospinning of biomaterial microfibers with potential for blended microfiber-cell-loaded gel composite structures, Adv. Healthc. Mater. 6 (2017), http://dx.doi.org/10.1002/adhm.201700456.
[25] A.L. Yarin, B. Pourdeyhimi, S. Ramakrishna, Fundamentals and Applications of Micro and Nanofibers, Cambridge University Press, Cambridge, 2014, http://dx.doi.org/10.1017/CBO9781107446830.
[26] C. Paredes, F.J. Martínez-Vázquez, A. Pajares, P. Miranda, Co-continuous calcium phosphate/polycaprolactone composite bone scaffolds fabricated by digital light processing and polymer melt suction, Ceram. Int. 47 (2021) 17726–17735, http://dx.doi.org/10.1016/J.CERAMINT.202103093.
[27] C. Ferrera, J.M. López-Herrera, M.A. Herrada, J.M. Montanero, A.J. Acero, Dynamical behavior of electrified pendant drops, Phys. Fluids. 25 (2013) 012104, http://dx.doi.org/10.1063/1.4776238.
[28] J.M. Montanero, A.M. Gañán-Calvo, Dripping, jetting and tip streaming, Rep. Prog. Phys. 83 (2020) 097001, http://dx.doi.org/10.1088/1361-6633/aba482.
[29] A.M. Gañán-Calvo, A. Barrero, C. Pantano-Rubiño, The electrohydrodynamics of electrified conical menisci, J. Aerosol Sci. 24 (1993) S19–S20, http://dx.doi.org/10.1016/0021-8502(93)90102-F.
[30] M.M. Denn, Continuous drawing of liquids to form fibres, Annu. Rev. Fluid Mech. 12 (1980) 365–387, http://dx.doi.org/10.1146/annurev.fl.12.010180.002053.
[31] F.H. Perera, F.J. Martínez-Vázquez, P. Miranda, A.L. Ortiz, A. Pajares, Clarifying the effect of sintering conditions on the microstructure and mechanical properties of β-tricalcium phosphate. Ceramics International 36 (2010) 1929-1935, https://doi.org/10.1016/j.ceramint.2010.03.015.
[32] C. Paredes, F.J. Martínez-Vázquez, H. Elsayed, P. Colombo, A. Pajares, P. Miranda, Evaluation of direct light processing for the fabrication of bioactive ceramic scaffolds: effect of pore/strut size on manufacturability and mechanical performance, J. Eur. Ceram. Soc. 41 (2021) 892–900, http://dx.doi.org/10.1016/J.JEURCERAMSOC.202009002.